Available online at www.sciencedirect.com

SciVerse ScienceDirect

Ceramics International 39 (2013) 5805–5811

CERAMICS INTERNATIONAL

www.elsevier.com/locate/ceramint

Synthesis and characterization of β-$Yb_2Si_2O_7$ powders

Cen Zhao[a,b], Feng Wang[a], Yinjie Sun[b], Yanchun Zhou[b,*]

[a]*Laboratory of Electrochemical Process and Technology for Materials, Beijing University of Chemical Technology, Beijing 100029, China*
[b]*Science and Technology of Advanced Functional Composite Laboratory, Aerospace Research Institute of Materials and Processing Technology, Beijing 100076, China*

Received 22 November 2012; received in revised form 24 December 2012; accepted 1 January 2013
Available online 12 January 2013

Abstract

β-$Yb_2Si_2O_7$ powders were synthesized by a sol–gel method using ytterbium nitrate and tetraethyl orthosilicate as starting materials. The thermal history, influence of composition and calcining temperature on phase evolution of the gel were investigated using TG–DTA, FTIR and X-ray diffraction. Amorphous $Yb_2Si_2O_7$ formed below 950 °C and a low-temperature phase (α-$Yb_2Si_2O_7$) was detected in powders calcined at 1000 °C and 1100 °C. Well crystalline β-$Yb_2Si_2O_7$ powders were obtained after calcining the xerogel at 1200 °C for 2 h. The average particle size of the powders calcined at 1200 °C was ~300 nm. The crystallite size determined from both TEM and FWHM of XRD reflections was ~60 nm. Lattice parameters of β-$Yb_2Si_2O_7$ determined by Rietveld method were $a=6.80053$ Å, $b=8.87508$ Å, $c=4.70740$ Å and $\beta=101.984°$. Atomic positions of β-$Yb_2Si_2O_7$ were identified as Yb(0.5, 0.80548, 0),Si(0.74150, 0.5, 0.42936), O(1) (0.5, 0.5, 0.5), O(2) (0.89831, 0.5, 0.75248), O(3) (0.74229, 0.65022, 0.18086).

Keywords: $Yb_2Si_2O_7$; Synthesis; Characterization; Powders

1. Introduction

Si-based nonoxide ceramics, including SiC and Si_3N_4, and Si-based ceramic matrix composites, are promising materials in applications such as structural parts for advanced engines, attributing to their superior high temperature mechanical properties and oxidation resistance in dry air [1,2]. However, the lack of environmental durability in combustion environments impedes the applications of these material [3]. To solve this problem, an environmental barrier coating (EBC) with good thermal and chemical stability, high melting point, excellent chemical and mechanical compatibility with Si-based ceramic matrix is employed to protect them from reacting with water vapor [4,5].

The earlier EBCs are based on mullite [6], mullite with YSZ (yttria-stabilized zirconia) [7] and BSAS (1-xBaO–xSrO–Al_2O_3–$2SiO_2$, $0 \le x \le 1$) overlay coats [8]. But in high temperature and high velocity combustion environment, these EBCs show either high recession rate or cracking and cannot meet the request to protect the matrix from corrosion by water vapor. Recent works have demonstrated that rare earth disilicates ($Re_2Si_2O_7$, Re = rare earth elements) with relatively low coefficient of thermal expansion (CTE) also have good phase stability and low recession rate in water vapor, making them promising as EBC candidates [4,9]. Many efforts have been put to prepare rare earth silicates. Among them, solid-state reaction [10,11], sol–gel synthesis [12,13] and hydrothermal synthesis [14] are three typical routes to prepare rare earth silicates powders. The advantages of sol–gel method include: First, the starting materials can be mixed at molecular scale; second, single phase powders can be obtained by controlling stoichiometric molar ratio of starting materials; and third the calcining temperature is usually 200–300 °C lower than that for solid-state reaction.

$Yb_2Si_2O_7$ is a candidate EBC for Si-based ceramics. Wang et al. [15] calculated water corrosion resistance of rare earth silicates by first-principles and gave the order of water corrosion resistance: $Yb_2Si_2O_7 > Sc_2Si_2O_7 > Y_2Si_2O_7 > Lu_2Si_2O_7$, which are consistent with the existing experimental results [9,16,17]. $Yb_2Si_2O_7$ is also a grain boundary phase of

*Corresponding author. Tel.: +86 10 68382478.
E-mail addresses: yczhou714@gmail.com, yczhou@imr.ac.cn (Y. Zhou).

0272-8842/$ - see front matter © 2013 Elsevier Ltd and Techna Group S.r.l. All rights reserved.
http://dx.doi.org/10.1016/j.ceramint.2013.01.001

Si_3N_4, which plays an important role on its high temperature mechanical properties [18,19] and thermal conductivities [20]. Hong et al. [21]found that the influence of rare-earth oxides on the strength retention of Si_3N_4 is in the sequence of Sm < Nd < Y < Yb. Despite of the unique properties of $Yb_2Si_2O_7$, the preparation and structure–property relationships have not been extensively investigated. Fernández-Carrión et al. [22] prepared $Yb_2Si_2O_7$ and $Yb_2Si_2O_7$–$Y_2Si_2O_7$ solid solutions using a sol–gel method and investigated the solid solubility of $Yb_2Si_2O_7$ in β-, γ- and δ-$Y_2Si_2O_7$. Beside this paper [22], seldom papers on the sol–gel synthesis of $Yb_2Si_2O_7$ can be found. Since the synthesis of phase-pure material is the first step to investigate the structure–property relationship, we prepared phase pure β-$Yb_2Si_2O_7$ powders by a sol–gel method in this work and analyzed the effect of initial composition and calcining temperature on their phase composition and morphology.

2. Experimental procedures

2.1. Synthesis of β-$Yb_2Si_2O_7$

$Yb(NO_3)_3 \cdot 6\,H_2O$ (99.95%, Rare-chem Co. Ltd, Huizhou,China), tetraethyl orthosilicate (TEOS) (AR, Sinopharm Chemical Reagent Co. Ltd., Shanghai, China), and C_2H_5OH (AR, Sinopharm Chemical Reagent Co. Ltd., Beijing, China) were used as starting materials for the synthesis of β-$Yb_2Si_2O_7$. Detailed process can be described as follows. First, $Yb(NO_3)_3 \cdot 6\,H_2O$ was dissolved in C_2H_5OH (molar ratio $Yb(NO_3)_3/C_2H_5OH = 1{:}10$) at 70 °C under continuously stirring for 1.5 h. Then the temperature of the solution was cooled down to room temperature (~25 °C). Stoichiometric amount of TEOS was dropwise added to the solution and the two starting materials were homogeneously mixed by stirring for 1 h. Then a small amount of 2 mol/L HCl (volume ratio $HCl/C_2H_5OH = 0.3\%$), which acted as catalyst, was added to the solution. The obtained solution was stirred in 70 °C oil bath for 8 h until a clear precursor sol formed. Finally, the sol was aged for about 60 h at room temperature and the gel was obtained.

Initially, we attempted to produce single-phase $Yb_2Si_2O_7$ with the stoichiometry of $Yb(NO_3)_3/TEOS = 1$. But Yb_2SiO_5 was always observed as impurity phase, which was attributed to the incompleteness of reactions or the volatilization of TEOS. As a result, five different sol samples with different $Yb(NO_3)_3 \cdot 6\,H_2O$ stoichiometric amount (molar ratio $Yb(NO_3)_3/TEOS = 1{:}0.9$, 1:1, 1:1.1, 1:1.2 and 1:1.3) were prepared and the rest of processing parameters were alike. The xerogels obtained from the five samples were calcined at various temperatures (1100 °C, 1200 °C and 1400 °C) and the X-ray diffraction patterns of calcined powders were analyzed, respectively. The phase composition were calculated by integrated intensity of XRD peaks as described by Chung [23–25] and the results are shown in Table 1. When the molar ratio of $Yb(NO_3)_3/TEOS$ is 1:1.2, the content of β-$Yb_2Si_2O_7$ is 96.4 wt% and ~100 wt% in powders calcined at 1200 °C and 1400 °C, respectively. Thus, we select the molar ratio $Yb(NO_3)_3/TEOS = 1{:}1.2$ to prepare β-$Yb_2Si_2O_7$ powders hereafter.

The wet gel was first dried in an oven at 60 °C for 10 h, then in a furnace at 200 °C for 1 h to get pale yellow xerogel. The xerogel was ground in an agate mortar to obtain fine powders before calcining in a furnace at different temperatures from 700 °C to 1200 °C for 2 h to investigate its evolution process and crystalline behavior.

2.2. Characterization of β-$Yb_2Si_2O_7$ powders

To investigate the thermal history of the gel, thermogravimetry and differential thermal analysis (TG-DTA, Thermoplus TG 8120, Rigaku, Japan) was conducted on the gel dried at 60 °C, which was heated in air at a rate of 10 °C/min from room temperature to 1400 °C. The weight and temperature changes were simultaneously recorded by a personal computer. Phase composition and phase evolution of the powders calcined at different temperatures were determined using infrared spectroscopy and X-ray diffraction analysis. The infrared spectra were recorded by Fourier transform infrared spectroscopy (FT-IR, Nicolet 8700/continuum XL, USA). X-ray diffraction analysis was conducted on an X-ray diffractometer (XRD, D8 advanced, Bruker, Germany) with Cu

Table 1
Phase component of powders at different temperatures.

Calcining temperature	1100 °C			1200 °C			1400 °C		
Phase composition (wt%)	α	β	*X*2	α	β	*X*2	α	β	*X*2
Yb/Si (molar ratio)									
0.9	0	78.9	21.1	0	80.5	19.5	0	82.7	17.3
1.0	0	83.9	16.1	0	89.0	11.0	0	89.3	10.7
1.1	18.8	67.1	14.1	0	95.4	4.6	0	96.8	3.2
1.2	29.4	58.9	11.7	0	96.4	3.6	0	~100	0
1.3	36.9	53.1	10.0	0	97.9	2.1	0	~100	0

α: α-$Yb_2Si_2O_7$, JCPDS card No. 30-1439.
β: β-$Yb_2Si_2O_7$, JCPDS card No. 25-1345.
*X*2: *X*2-Yb_2SiO_5, JCPDS card No. 40-0386.

K_α radiation ($\lambda = 1.54178$ Å). The phase compositions were analyzed by Jade 5.0 software (Material data Inc., USA) and the lattice parameters, atomic positions, 2θ, $h\,k\,l$ and peak intensities of β-$Yb_2Si_2O_7$ were refined by the Rietveld method [26,27] (Topas software, Bruker, Germany). The reliability factor R_p and R_{wp} were calculated by

$$R_p = \frac{\sum_i \left| cY^{\mathrm{sim}}(2\theta_i) - I^{\mathrm{exp}}(2\theta_i) + Y^{\mathrm{back}}(2\theta_i) \right|}{\sum_i \left| I^{\mathrm{exp}}(2\theta_i) \right|} \quad (1)$$

$$R_{wp} = \left(\frac{[\sum_i w_i (cY^{\mathrm{sim}}(2\theta_i) - I^{\mathrm{exp}}(2\theta_i) + Y^{\mathrm{back}}(2\theta_i))^2]}{\sum_i w_i (I^{\mathrm{exp}}(2\theta_i))^2} \right)^{1/2} \quad (2)$$

where $w_i = 1/I^{\mathrm{exp}}(2\theta_i)$ is a weighting function, c the constant scaling factor optimized to obtain the lowest value of R_{wp}, $I^{\mathrm{exp}}(2\theta_i)$ the measured experimental spectrum, $Y^{\mathrm{back}}(2\theta_i)$ the background intensity of the measured spectrum, and $Y^{\mathrm{sim}}(2\theta_i)$ the simulated diffraction intensity without the background contribution. The intensity was calculated by

$$I_{\mathrm{Rietveld}}(2\theta) = b(2\theta) + S\sum_k L_k |F_k|^2 \phi(2\theta_i - 2\theta_k) P_k A_k \quad (3)$$

where $b(2\theta)$ is the background intensity, S the scale factor, L_k contains the Lorentz polarization and multiplicity factors, ϕ the profile function, P_k the preferred orientation function, A_k absorption factor, and F_k the structure factor. The index k presents Miller indices for the Bragg reflections. The average crystallite size was calculated using Scherer's equation:

$$D = \frac{0.89\lambda}{\beta \cos\theta} \quad (4)$$

where D is the average crystallite size in nm, λ the wavelength of Cu K_α radiation, β the corrected full-width at half-maximum in radian (FWHM), and θ the diffraction peak angle. The particle size, crystallite size and powder morphology were investigated by a laser particle size analyzer (Nano ZS90, Malvern, UK), a scanning electron microscope (FE-SEM, JSM-6701F, JEOL, Japan) and a transmission electron microscope (TEM, Tecnai G^2, FEI company, the Netherland) working at an accelerating voltage of 200 kV.

3. Results and discussion

3.1. Thermal analysis

To clarify thermal history of the gel during heating, the gel dried at 60 °C was chosen for the TG–DTA analysis and the curves are shown in Fig. 1. The endothermic peak at 128.9 °C is assigned to the evaporation of weakly bonded molecules, such as water and ethanol molecules. The weight loss in the temperature range 20–130 °C is about 31%, demonstrating that there are still a large amount of water and ethanol molecules in the gel network after drying at 60 °C for 10 h. The endothermic peak at 377.6 °C is attributed to the pyrolysis of nitrates and the removal of strong bonded water molecules, with a weigh loss of about 19%. The broad exothermic peak at temperature range 500–1000 °C may correspond to the formation of amorphous $Yb_2Si_2O_7$. The weak endothermic peak at 1052.2 °C corresponds to the formation of β-$Yb_2Si_2O_7$, indicating a phase transformation from α-$Yb_2Si_2O_7$ to β-$Yb_2Si_2O_7$, which is confirmed by XRD analysis. There is almost no weight loss and no endothermic or exothermic peaks detected in a temperature range 1200–1400 °C, demonstrating the good thermal stability of $Yb_2Si_2O_7$.

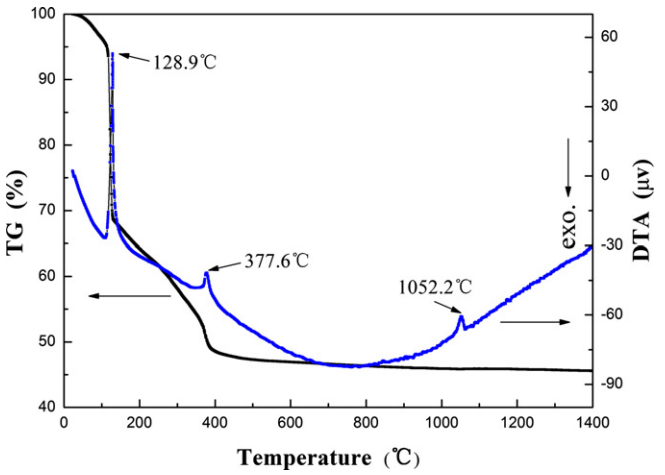

Fig. 1. Simultaneous TG–DTA curves of gel dried at 60 °C for 10 h.

3.2. X-ray diffraction analysis

To demonstrate the phase evolution and phase composition of powders, the XRD patterns of xerogel and powders calcined at several temperatures from 700 °C to 1400 °C are shown in Fig. 2(a) and (b). The xerogel dried at 200 °C shows amorphous state, indicating the existence of polymeric network. The broad peaks at $2\theta = 21°$ and $2\theta = 30°$ in XRD patterns of powders calcined at 700 °C, 900 °C and 950 °C indicate that the powders are in amorphous state. Crystalline peaks are observed in powders calcined above 1000 °C. At 1000 °C and 1100 °C, the phase composition of powders includes $X2$-Yb_2SiO_5 that crystallize in monoclinic structure with a space group $I2/a$ (JCPDS card No. 40-0386), α-$Yb_2Si_2O_7$ that crystallize in triclinic structure with a space group $P1$ (JCPDS card No. 30-1439) and β-$Yb_2Si_2O_7$ that crystallize in monoclinic structure with a space group $C2/m$ (JCPDS card No. 25-1345). When the calcining temperature increases to 1200 °C, the phase transformation from α-$Yb_2Si_2O_7$ to β-$Yb_2Si_2O_7$ completes and only β-$Yb_2Si_2O_7$ can be clearly detected with a little amount $X2$-Yb_2SiO_5 (3.6 wt% in Table 1) as an impurity phase. No other high-temperature phase can be detected at the calcining temperature of 1400 °C, which proves that β-$Yb_2Si_2O_7$ is stable at this temperature. The above XRD phase composition analysis proves that sol–gel method is a suitable one to prepare ytterbium disilicate at a lower calcining temperature comparing with solid-state synthesis (calcining Yb_2O_3 and SiO_2 powders at 1500 °C [28]) and phase pure β-$Yb_2Si_2O_7$ can be prepared by controlling the molar ratio of starting materials.

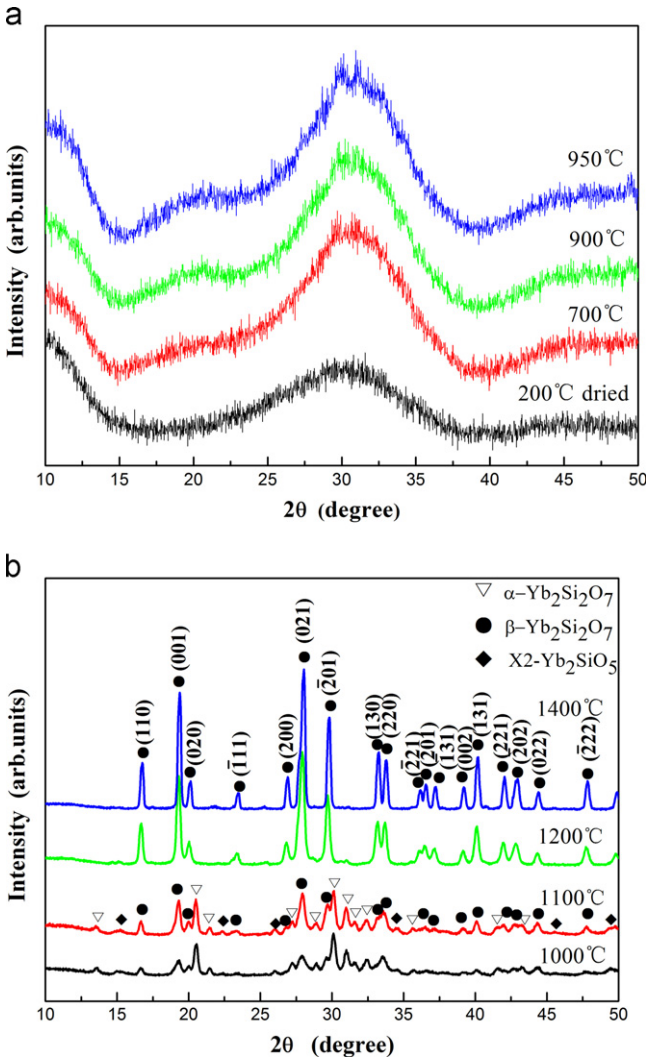

Fig. 2. XRD patterns of powders calcined at various temperatures. (a) 200–950 °C, (b) 1000–1400 °C.

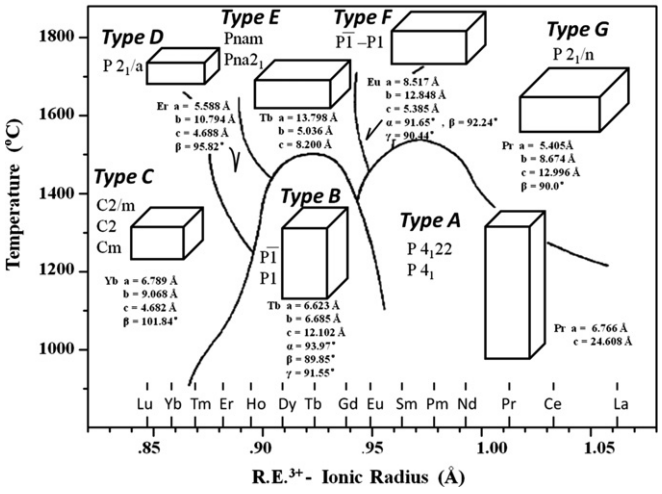

Fig. 3. Crystal data on the structure types A–G of rare-earth disilicates compounds.

In previous work of Fernández-Carrión et al., [22] no α-$Yb_2Si_2O_7$ was observed in the calcined powders, which can be explained by the fact that only higher calcining temperature (> 1200 °C) was used. In our present work we used several calcining temperature from 700 °C to 1400 °C to investigate the phase evolution process. Thus low temperature α-$Yb_2Si_2O_7$ phase was detected in powders calcined at 1000–1100 °C. It is well known that the polymorphism of rare-earth disilicates is influenced by rare-earth cation size, temperature and pressure. From the polymorphism of rare-earth disilicates $Re_2Si_2O_7$ versus temperature diagram at atmospheric pressure (Fig. 3) [24], it can be seen that β-$Yb_2Si_2O_7$ with monoclinic structure is the only stable phase from 1000 °C to about 1600 °C. While α-type $Re_2Si_2O_7$ phases are usually detected in large size rare-earth disilicates like $Ho_2Si_2O_7$, $Dy_2Si_2O_7$ and $Tb_2Si_2O_7$. However, in our work α-$Yb_2Si_2O_7$ with a triclinic structure coexists with β-$Yb_2Si_2O_7$ at 1000–1100 °C. The presence of diverse polymorphisms in $Yb_2Si_2O_7$ demonstrates that the crystal structure of $Yb_2Si_2O_7$ is strongly dependent on the thermal history and preparation methods of the material. The observed phenomenon also enriches our knowledge to $Yb_2Si_2O_7$ and more work is needed to understand the formation mechanism of α-$Yb_2Si_2O_7$ at relatively low temperatures.

To further confirm the sol–gel synthesized and 1200 °C calcined powders are β-$Yb_2Si_2O_7$, Rietveld method was conducted to validate XRD data. The reliability factors calculated from Eqs. (1) and (2) are $R_p = 7.29\%$ and $R_{wp} = 9.37\%$, respectively. The refined lattice parameters are $a = 6.80053$ Å, $b = 8.87508$ Å, $c = 4.70740$ Å and $\beta = 101.984°$, which agree well with the lattice parameters given in JCPDS card No. 25-1345 ($a = 6.80200$ Å, $b = 8.87500$ Å, $c = 4.70300$ Å, $\beta = 102.120°$). The atomic positions of β-$Yb_2Si_2O_7$ are identified as Yb(0.5, 0.80548, 0),Si(0.74150, 0.5, 0.42936), O(1) (0.5, 0.5, 0.5), O(2) (0.89831, 0.5, 0.75248), O(3) (0.74229, 0.65022, 0.18086), and are compared in Table 2 with the data from J. Fleche's work [29]. The calculated and experimental data of reflections, 2θ and intensities (calculated by Eq. (3)) of β-$Yb_2Si_2O_7$ are presented in Table 3. The data from JCPDS card are also given for comparison. For β-$Yb_2Si_2O_7$ powders, 2θ and peak intensities are well consistent with the calculated and JCPDS card data, which proves that the powders obtained after calcining at 1200 °C, are β-$Yb_2Si_2O_7$.

The crystallite size of β-$Yb_2Si_2O_7$ calcined at 1200 °C was calculated from the FWHM of (0 0 1), (0 2 0) and (2 0 0) diffraction peaks using Eq. (4). The results are 60.2 nm, 59.9 nm and 57.9 nm, respectively, indicating that the β-$Yb_2Si_2O_7$ crystallites are equa axis with average size of ~59 nm. The crystallite size of β-$Yb_2Si_2O_7$ calcined at 1400 °C calculated from the FWHM of (0 0 1), (0 2 0) and (2 0 0) are 68.4 nm, 68.4 nm and 68.8 nm, respectively, which proves that the crystallite size of powders increases with the calcining temperature.

3.3. FTIR analysis

To further confirm the weight loss from 20 °C to 130 °C is from evaporation of water and ethanol molecules and the

powders calcined at 1200 °C are β-$Yb_2Si_2O_7$, FTIR was conducted. Fig. 4 shows the FTIR spectra of xerogel powders dried at 200 °C for 1 h and the powders calcined at 1200 °C. β-$Yb_2Si_2O_7$ have similar crystal structure with β-$Y_2Si_2O_7$, so we use previous FTIR spectra of β-$Y_2Si_2O_7$ for comparation. The peak at 1676 cm^{-1} in curve (a) originates from the deformation vibration of H_2O. The absorption bands at 1570 cm^{-1}, 1465 cm^{-1}, 1327 cm^{-1}, 1030 cm^{-1} are assigned to the bending mode of $–CH_3$ and $–CH_2$, the stretching vibration of C–O, the stretching vibration of C–C, respectively, indicating the existence of ethanol molecules and alkoxy groups in the xerogel. The asymmetric and symmetric stretching vibration of Si–O corresponds to the peaks at 813 cm^{-1} and 755 cm^{-1} [30]. And the peak at 460 cm^{-1} is attributed to the bending mode of Yb–OH [31]. Thus it is obvious that the weight loss from 20 °C to 130 °C is from evaporation of water and ethanol molecules.

As shown in curve (b) of Fig. 4, the peaks at 1133 cm^{-1} and 1108 cm^{-1} are ascribed to the stretching vibration of silicon atoms against oxygen atoms in Si–O–Si bond. The remaining high-frequency modes correspond to Si–O stretching motion involving apical (non-bridging) oxygen atoms. In particular, we have assigned the peak located at 983 cm^{-1} to stretching modes involving an oxygen atom coordinated to two ytterbium atoms defining a line normal to the Si–O–Si chain, and 912 cm^{-1} to similar modes involving two ytterbium atoms in a line subparallel to the Si–O–Si chain. The peak at 853 cm^{-1} is the multiple stretching modes of Si–O bands [32]. The peaks

Table 2
Crystal structure parameters for β-$Yb_2Si_2O_7$.

Space group	*C*2/*m*	
Structure parameters	JCPDS card No. 25-1345	Rietveld refined
a (Å)	6.80200	6.80053
b (Å)	8.87500	8.87508
c (Å)	4.70300	4.70740
β(°)	102.120	101.984
Atomic positions	Ref [29]	
Yb	(0.5, 0.80687(2), 0)	(0.5, 0.80548, 0)
Si	(0.7189(3), 0.5, 0.4125(6))	(0.74150, 0.5, 0.42936)
O(1)	(0.5, 0.5, 0.5)	(0.5, 0.5, 0.5)
O(2)	(0.8831(5), 0.5, 0.7151(15))	(0.89831, 0.5, 0.75248)
O(3)	(0.7361(5),0.6504(4),0.2197(11))	(0.74229, 0.65022, 0.18086)

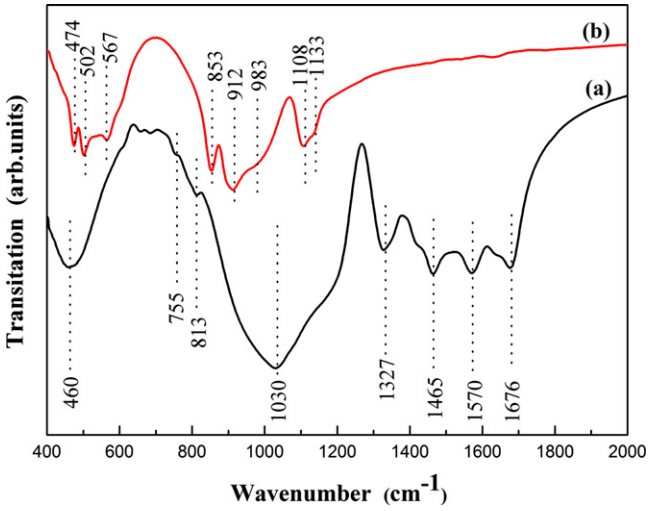

Fig. 4. FT-IR spectra of (a) xeogel dried at 200 °C (b) calcined powders at 1200 °C.

Table 3
Reflections, 2θ, and intensities data of β-$Yb_2Si_2O_7$ from calculation (Cal.), experiment (Obs.) and JCPDS card No. 25-1345.

Reflection (*h k l*)	$2\theta_{Cal.}$ (°)	$2\theta_{Obs.}$ (°)	$2\theta_{JCPDS.}$ (°)	$I/I_{oCal.}$ (%)	$I/I_{oObs.}$ (%)	$I/I_{oJCPDS.}$ (%)
(1 1 0)	16.64	16.70	16.64	26.9	37.6	43
(0 0 1)	19.26	19.30	19.29	66.1	79.7	87
(0 2 0)	20.00	20.04	19.99	16.1	20.7	28
($\bar{1}$ 1 1)	23.33	23.36	23.33	10.6	10.2	11
(2 0 0)	26.78	26.84	26.79	22.9	16.2	25
(1 1 1)	27.63	–	27.66	27.8	–	35
(0 2 1)	27.91	27.92	27.92	100.0	100.0	100
($\bar{2}$ 0 1)	29.66	29.70	29.65	58.8	61.7	61
(1 3 0)	33.12	33.20	33.11	39.8	38.4	44
(2 2 0)	33.65	33.70	33.65	36.0	37.6	34
($\bar{2}$ 2 1)	36.03	36.14	36.01	10.9	12.7	13
(2 0 1)	36.44	36.44	36.50	16.2	15.0	16
($\bar{1}$ 3 1)	37.09	37.18	37.09	14.7	15.1	16
(0 0 2)	39.10	39.16	39.15	13.3	11.4	12
(1 3 1)	40.06	40.12	40.08	37.7	33.9	32
(0 4 0)	40.64	–	40.62	2.4	–	2
(2 2 1)	41.91	41.98	41.95	18.4	16.9	20
($\bar{3}$ 1 1)	42.62	–	42.59	14.7	–	10
($\bar{2}$ 0 2)	42.84	42.84	42.82	14.4	16.8	15
(0 2 2)	44.30	44.34	44.35	12.9	10.3	10
($\bar{2}$ 2 2)	47.71	47.72	47.70	14.6	16.6	16

at 567 cm^{-1} and 502 cm^{-1} are attributed to the stretching vibration of Yb–O bonds [22], and the bending mode of Yb–OH is observed at 474 cm^{-1} [33]. The above results further demonstrate the powders calcined at 1200 °C are β-$Yb_2Si_2O_7$.

3.4. Particle size distribution, SEM and TEM observation of β-$Yb_2Si_2O_7$ powders

Powder morphology and particle size play an important role in both sintering of bulk sample and coating on composite materials. To characterize the particle size and morphology of $Yb_2Si_2O_7$, β-$Yb_2Si_2O_7$ powders calcined at 1200 °C and ball milled for 1 h were analyzed by using SEM and laser particle size analyzer. Fig. 5 illustrates the morphology of β-$Yb_2Si_2O_7$ powders. The powders are well crystalline with an average particle size of about 300 nm. Within the β-$Yb_2Si_2O_7$ particles, there are a number of nanoparticles of 30–100 nm in size. The 1 wt% suspension used for size distribution measurement was prepared by adding a certain amount of as-received β-$Yb_2Si_2O_7$ powder to deionized water. The suspension was then ultrasonically deflocculated (SB-5200, Scientz biotechnology Co. Ltd., Ningbo, China) at an output power of 160 W in an ice bath. After ultrasonication, the suspension was stirred continuously before analysis. The average particle size of well-dispersed powder determined by a laser particle size analyzer is 318 nm, which agrees with the SEM results. The inset in Fig. 5 shows the particle size of powders is distributed over a broad range (43–2669 nm).

To further confirm the sol–gel synthesized and calcined powders are $Yb_2Si_2O_7$ and give insight on the microstructure of β-$Yb_2Si_2O_7$ powders, TEM analysis of $Yb_2Si_2O_7$ powders were performed. Fig. 6 shows the TEM micrographs of $Yb_2Si_2O_7$ powders calcined at 1200 °C. The overview of powders (Fig. 6(a)) shows no agglomeration with several crystallites in each particle. Fig. 6(b) illustrates several sets of lattice fringes oriented in different directions, confirming that there are several crystallites in a particle and the powders are highly crystalline after 2 h calcining at 1200 °C. The d-spacings measured from the image are 0.330 nm, 0.320 nm and 0.230 nm, and they can be assigned to the d-spacings of (2 2 0), (1 1 1) and (0 0 2) planes of β-$Yb_2Si_2O_7$, respectively. The estimate size of crystallites from Fig. 6(b) is ~60 nm, which is quite consistent with that from XRD analysis.

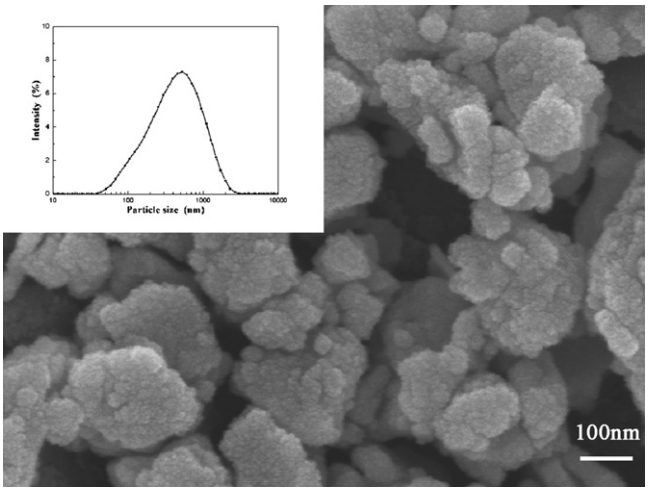

Fig. 5. SEM image and size distribution of β-$Yb_2Si_2O_7$ powders.

4. Conclusions

β-$Yb_2Si_2O_7$ powders were successfully prepared by a sol–gel method using $Yb(NO_3)_3 \cdot 6H_2O$ and TEOS as initial materials. The molar ratio of $Yb(NO_3)_3 \cdot 6H_2O$ to TEOS and calcining temperature have great influence on the crystallinity and phase composition of the powders. Investigations based on TG–DTA, FTIR and XRD revealed the thermal history and phase evolution of the gel during heating. Crystalline $Yb_2Si_2O_7$ powders, which were a mixture of α-$Yb_2Si_2O_7$ and β-$Yb_2Si_2O_7$, formed at 1000 °C. A phase transformation from α-$Yb_2Si_2O_7$ to β-$Yb_2Si_2O_7$ was observed during calcining process in the temperature range 1000–1200 °C. β-$Yb_2Si_2O_7$ powders were obtained after calcining xerogel at 1200 °C for 2 h. The powders are of ~300 nm in particle size with crystallites of ~60 nm within the particles.

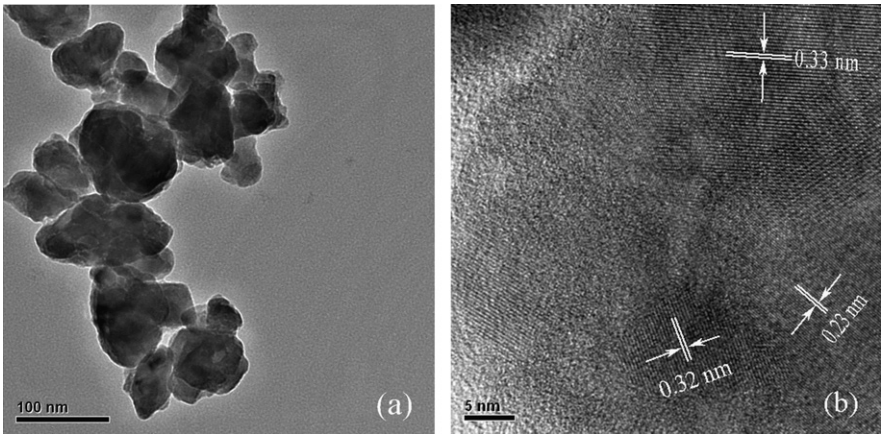

Fig. 6. TEM micrographs of calcined $Yb_2Si_2O_7$ powders (a) an overview image, (b) several gains in a particle.

Acknowledgement

This work was supported by the National Outstanding Young Scientist Foundation (No. 59925208 for Y.C. Zhou), Natural Science Foundation of China under Grant No. 50832008 and No.91226202.

References

[1] R. Raj, Fundamental research in structural ceramics for service near 2000 °C, Journal of the American Ceramic Society 76 (1993) 2147–2174.
[2] R. Riedel, H. Kleebe, H. Schönfelder, F. Aldinger, A covalent micro/nano-composite resistant to high-temperature oxidation, Nature 374 (1994) 526–528.
[3] J.L. Smialek, R.C. Robinson, E.J. Opila, D.S. Fox, N.S. Jacobson, SiC and Si_3N_4 recession due to SiO_2 scale volatility under combustor conditions, Advanced Composite Materials 8 (1999) 33–45.
[4] K.N. Lee, D.S. Fox, N.P. Bansal, Rare earth silicate environmental barrier coatings for SiC/SiC composites and Si_3N_4 ceramics, Journal of the European Ceramic Society 25 (2005) 1705–1715.
[5] S. Ueno, T. Ohji, H. Lin, Recession behavior of a silicon nitride with multi-layered environmental barrier coating system, Ceramics International 33 (2007) 859–862.
[6] K.N. Lee, R.A. Miller, N.S. Jabocson, New generation of plasma-sprayed mullite coatings on silicon-carbide, Journal of the American Ceramic Society 78 (1995) 705–710.
[7] K.N. Lee, R.A. Miller, Durability of Mulliter YSZ-coated SiC in 90% H_2O–O_2, Advances in Ceramic Matrix Composites IV, The American Ceramic Society, Westerville, OH, 1999, pp. 17–25.
[8] K.N. Lee, Current status of environmental barrier coatings for Si-based ceramics, Surface and Coatings Technology 133-134 (2000) 1–7.
[9] N. Maier, K.G. Nickel, G. Rixecker, High temperature water vapor corrosion of rare earth disilicates $(Y,Yb,Lu)_2Si_2O_7$ in the presence of $Al(OH)_3$ impurities, Journal of the European Ceramic Society 27 (2007) 2705–2713.
[10] H.T. Sun, M. Fujii, N. Nitta, F. Shimaoka, M. Mizuhata, H. Yasuda, S. Deki, S. Hayashi, Large-scale controllable synthesis and characterization of ytterbium silicate nanostructures, Journal of the American Ceramic Society 91 (2008) 4158–4161.
[11] Z.Q. Sun, Y.C. Zhou, M.S. Li, Low-temperature synthesis and sintering of γ-$Y_2Si_2O_7$, Journal of Materials Research 21 (2006) 1443–1450.
[12] D. Boyer, B. Derby, Yttrium silicate powers produced by the sol–gel method, structural and thermal characterization, Journal of the American Ceramic Society 86 (2003) 1595–1597.
[13] H.M. Wen, S.M. Dong, P. He, Z. Wang, H.J. Zhou, X.Y. Zhang, Sol–gel synthesis and characterization of ytterbium silicate powers, Journal of the American Ceramic Society 90 (2007) 4043–4046.
[14] X.P. Tang, Y.F. Gao, H.F. Chen, H.J. Luo, Hydrothermal synthesis of lutetium disilicate nanoparticles, Journal of Solid State Chemistry 188 (2012) 38–43.
[15] Y.G. Wang, J.L. Liu, First-principles investigation on the corrosion resistance of rare earth disilicates in water vapor, Journal of the European Ceramic Society 29 (2009) 2163–2167.
[16] S. Ueno, T. Ohji, H.T. Lin, Designing lutetium silicate environmental barrier coatings for silicon nitride and its recession behavior in steam jets, Journal of Ceramic Processing Research 7 (2006) 20–23.
[17] T. Ohji, Environmental barrier coating on silicon nitride; challenges and critical issues, in: Proceedings of the 28th Int. Conf. & Exp. On Adv. Ceram. & Composites, 2004.
[18] W.-H. Lee, H.-E. Kim, S.-J. Cho, Microstructural evolution of gas-pressure-sintered Si_3N_4 with Yb_2O_3 as a sintering aid, Journal of the American Ceramic Society 80 (1997) 2737–2740.
[19] H. Park, H.-E. Kim, Microstructural evolution and mechanical properties of Si_3N_4 with Yb_2O_3 as a sintering additive, Journal of the American Ceramic Society 8 (1997) 750–756.
[20] H. Miyazaki, Y. Yoshizawa, K. Hirao, Fabrication of high thermal-conductive silicon nitride ceramics with low dielectric loss, Materials Science and Engineering, B 161 (2009) 198–201.
[21] Z.L. Hong, H. Yoshida, Y. Ikuhara, T. Sakuma, T. Nishimura, M. Mitomo, The effect of additives on sintering behavior and strength retention in silicon nitride with RE-disilicate, Journal of the European Ceramic Society 22 (2002) 527–534.
[22] A.J. Fernández-Carrión, M.D. Alba, A. Escudero, A.I. Becerro, Solid solubility of $Yb_2Si_2O_7$ in β-, γ- and δ-$Y_2Si_2O_7$, Journal of Solid State Chemistry 184 (2011) 1882–1889.
[23] F.H. Chung, Quantitative interpretation of X-ray diffraction patterns of mixtures. I. Matrix-flushing method for quantitative multicomponent analysis, Journal of Applied Crystallography 7 (1974) 519–525.
[24] F.H. Chung, Quantitative interpretation of X-ray diffraction patterns of mixtures. II. Adiabatic principle of X-ray diffraction analysis of mixtures, Journal of Applied Crystallography 7 (1974) 526–531.
[25] F.H. Chung, Quantitative interpretation of X-ray diffraction patterns of mixtures. III. Simultaneous determination of a set of reference intensities, Journal of Applied Crystallography 8 (1975) 17–19.
[26] H.M. Rietveld, Line profiles of neutron powder-diffraction peaks for structure refinement, Acta Crystallographica 22 (1967) 151–152.
[27] H.M. Rietveld, A profile refinement method for nuclear and magnetic structures, Journal of Applied Crystallography 2 (1969) 65–71.
[28] S. Ueno, T. Ohji, H. Lin, Recession behavior of $Yb_2Si_2O_7$ phase under high speed steam jet at high temperatures, Corrosion Science 50 (2008) 178–182.
[29] J. Fleche, The crystal chemistry of the rare-earth silicates, Structure and Bonding 13 (1973) 99–197.
[30] A. Bertoluzza, C. Fagnano, M.A. Morelli, V. Gottardi, M. Guglielmi, Raman and infrared spectra on silica gel evolving towards glass, Journal of Non-Crystalline Solids 48 (1982) 117–128.
[31] X. Wang, L. Andrews, Infrared spectra and density functional calculations for $M(OH)_{2,3}$ and HOMO molecules and $M(OH)_2^+$ cations (M=Y, La), Journal of Physical Chemistry A 110 (2006) 4157–4168.
[32] M. Diaz, C. Pecharroman, F. del Monte, J. Sanz, J.E. Iglesias, J.S. Moya, C. Yamagata, S. Mello-Castano, Synthesis, thermal evolution, and luminescence properties of yttrium disilicate host matrix, Chemistry of Materials 17 (2005) 1774–1782.
[33] Z.Q. Sun, X.W. Zhu, M.S. Li, Y.C. Zhou, Y. Sakka, Hydrolysis and dispersion properties of aqueous γ-$Y_2Si_2O_7$ suspension, Journal of the American Ceramic Society 92 (2009) 54–61.